Examining Substrate-Induced Plasmon Mode Splitting and Localization in Truncated Silver Nanospheres with Electron Energy Loss Spectroscopy

8 **AUTHORS**, INCLUDING:

Guoliang Li
University of Notre Dame
8 PUBLICATIONS   **48** CITATIONS

SEE PROFILE

Charles Cherqui
University of Washington Seattle
15 PUBLICATIONS   **15** CITATIONS

SEE PROFILE

Nicholas W Bigelow
University of Washington Seattle
10 PUBLICATIONS   **144** CITATIONS

SEE PROFILE

Examining Substrate-Induced Plasmon Mode Splitting and Localization in Truncated Silver Nanospheres with Electron Energy Loss Spectroscopy

Guoliang Li,[†,¶] Charles Cherqui,[‡,¶] Yueying Wu,[§] Nicholas W. Bigelow,[‡] Philip D. Simmons,[∥] Philip D. Rack,[§,⊥] David J. Masiello,*[‡] and Jon P. Camden*[†]

[†]Department of Chemistry and Biochemistry, University of Notre Dame, Notre Dame, Indiana 46556, United States
[‡]Department of Chemistry, University of Washington, Seattle, Washington 98195, United States
[§]Department of Materials Science and Engineering, University of Tennessee, Knoxville, Tennessee 37996, United States
[∥]Department of Chemistry, University of Tennessee, Knoxville, Tennessee 37996, United States
[⊥]Center for Nanophase Materials Sciences, Oak Ridge National Laboratory, Oak Ridge, Tennessee 37831, United States

Ⓢ *Supporting Information*

ABSTRACT: Motivated by the need to study the size dependence of nanoparticle–substrate systems, we present a combined experimental and theoretical electron energy loss spectroscopy (EELS) study of the plasmonic spectrum of substrate-supported truncated silver nanospheres. This work spans the entire classical range of plasmonic behavior probing particles of 20–1000 nm in diameter, allowing us to map the evolution of localized surface plasmons into surface plasmon polaritons and study the size dependence of substrate-induced mode splitting. This work constitutes the first nanoscopic characterization and imaging of these effects in truncated nanospheres, setting the stage for the systematic study of plasmon-mediated energy transfer in nanoparticle–substrate systems.
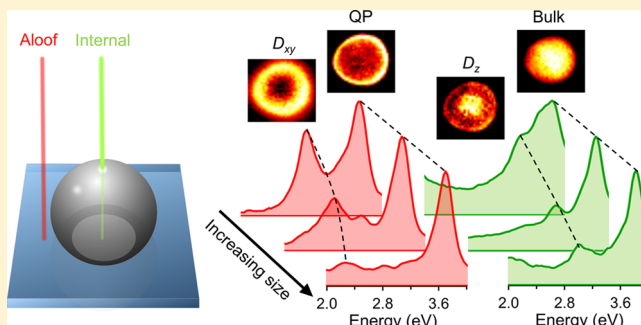
Localized surface plasmon resonances (LSPRs) are the coherent and collective oscillations of conduction band electrons at the surface of metallic nanoparticles. LSPRs are known to localize far-field light to a subdiffraction-limited length scale, yielding an intense electric field at the particle surface. This effect has been harnessed to dramatically enhance light–matter interactions, leading to a variety of applications such as surface-enhanced Raman spectroscopy (SERS),[1,2] subwavelength waveguides,[3] plasmonically enhanced photovoltaics (PV),[4,5] and photocatalysis.[6,7] The broad field of interest that employs the use and study of LSPRs is known as plasmonics, which is expected to be a critical technology in the merging of photonics and electronics toward nanoscale dimensions.[8]

Despite several important milestones,[9–13] the potential of LSPRs in enhancing solar energy-harvesting efficiency has yet to be realized.[14] Though a myriad of reasons exist, the most significant obstacle is the incomplete description of energy transfer between the LSPR and the neighboring environment. Plasmon-mediated energy transfer can be accomplished via two often-competing pathways: (1) plasmon-induced electron transfer and (2) plasmon-induced resonance energy transfer,[15–18] and it is challenging to distinguish them from each other in experiment. Recently, it was shown that the efficiency of plasmon-mediated energy transfer can be controlled by

varying the parameters of the system, such as the particle geometry or the optoelectronic properties of the substrate.[15,17–21] Electron energy loss spectroscopy (EELS) performed in a scanning transmission electron microscope (STEM) has also revealed that substrate-induced LSPR localization can be manipulated to tune the efficiency of energy transfer in nanocube–substrate systems.[15] These studies indicate that energy transfer is highly dependent on the interplay between LSPRs and the electronic structure of the substrate. Because the spatial and energetic profiles of LSPRs can be tuned by varying the particle size,[22–24] it is tempting to conduct a full-size study of the nanocube-substrate system to gain a deeper understanding of plasmon-mediated energy transfer. However, because nanocubes are only available in a limited size range (<200 nm in cube edge length),[25,26] it is necessary to pursue alternative systems which exhibit similar LSPR localization effects but do not suffer from particle-size restrictions.

Another system which exhibits strong interface localization[19,27,28] and has generated significant interest is the

substrate-supported truncated nanosphere. This system has recently been used to spatially manipulate electron transfer in photocatalytic and PV applications,[19,29−33] in addition to other novel effects such as the plasmonic control of particle morphology[19,34] and plasmon-induced nanoscale heating.[35] Despite the fascinating properties of substrate-supported truncated nanospheres, a near-field characterization of their LSPR modes, including size dependence, is still lacking. Unlike nanocubes, substrate-supported truncated nanospheres can be synthesized over the nanometer-to-micron length scales via pulsed laser-induced dewetting (PLiD).[36−39] This method produces a distribution of particles with remarkably smooth surfaces and nearly identical geometry, setting the stage for the systematic study of their plasmonic properties.

In this paper, we present a combined experimental and theoretical EELS study of the plasmonic spectrum of PLiD synthesized truncated Ag nanospheres on a 30 nm thick silicon nitride (Si_3N_4) substrate, spanning the entire classical range of plasmonic behavior for particles of diameter $d = 20-1000$ nm. We identify all LSPR modes supported by the system, map out their spatial profiles, and present the first three-dimensional (3D) characterization of LSPR mode splitting in single truncated nanospheres. The size span investigated here enables us to visualize, for the first time, the spatial and spectral evolution of an LSPR into a surface plasmon polariton (SPP). The experiments are interpreted in the context of Mie theory and full-wave electrodynamics simulations using both the photon- and electron-driven discrete dipole approximations (DDA[40] and e-DDA[41,42]). The schematic of the EELS experimental setup is shown in Figure 1a. The cross section Z-contrast image of the truncated Ag nanospheres sitting on a Si_3N_4 substrate is shown in Figure 1b.
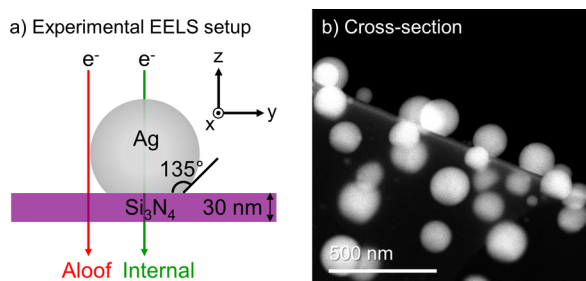

Figure 1. (a) Schematic of the experimental EELS setup. All Ag nanoparticles are supported by a 30 nm thick Si_3N_4 substrate with a contact angle of 135°. Both aloof (red) and internal (green) beam trajectories are considered in this study. (b) Cross section Z-contrast images of the Ag nanoparticles on Si_3N_4 substrate.

Many previous studies have relied on far-field optical probes to examine similar systems and have reported plasmon mode splitting in truncated nanospheres.[19,27,28] However, due to the limited spatial resolution of these methods, prior measurements were unable to experimentally characterize the spatial profile of the modes, a task to which STEM/EELS is exceptionally well suited. Additionally, owing to the selection-rules imposed by the optical probe, only the bright modes can be excited. By contrast, due to the localized nature of the electron probe, it has the ability to excite both bright and dark modes. Although STEM/EELS experiments have examined substrate supported hemispheres ranging from $d = 1-20$ nm, that work was limited in scope by the energy resolution of the electron probe and focused mainly on quantum size effects.[43,44] Since then, state-

of-the-art STEM/EELS has greatly improved its space and energy resolving capabilities,[45] and it is now possible to measure both the spectral and spatial profiles of all LSPR modes supported by the system.[46] More recently, EELS was used to study quantum size effects in nanospheres without truncation, minimizing the role of the substrate in comparison to the system studied here.[23]

The intuition derived from Mie theory[47] provides a basis for understanding the plasmon modes of the substrate-supported truncated sphere. We therefore begin our discussion with a brief overview of Mie theory. The LSPR modes of a spherical particle are characterized by an angular momentum number l, the value of which determines several interesting properties of the mode in question. Odd-mode number LSPRs have a nonzero net dipole moment and couple to the radiation field, making them "bright" modes. Even-mode number LSPRs have a zero net dipole moment and do not couple to the radiation field, making them "dark" modes. Aside from the brightness of the mode, l also gives the number of nodes in the electric field along the surface of the nanosphere.[48,49] The radial component of the electric field at an observation point r scales as r^{l-1} inside and $r^{-(l+2)}$ outside of the sphere; therefore, as l increases, the electric field becomes increasingly bound to the surface.

The range of angular momentum states (l-modes) supported by the sphere is a function of particle diameter and the maximum l achievable increases with size. With large enough l, the LSPR becomes indistinguishable from a standing wave SPP. This evolution is illustrated explicitly in Figure 2, which displays
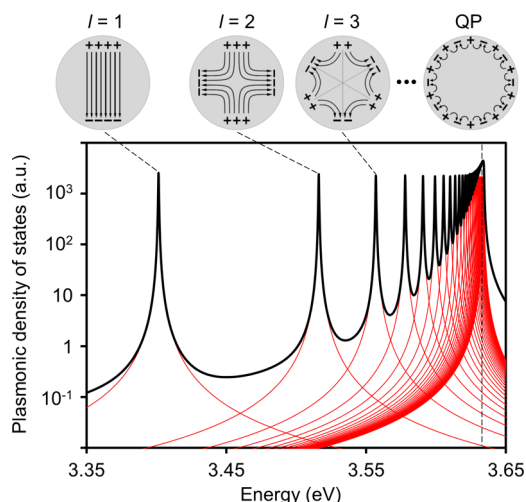

Figure 2. Plasmonic density of states of a perfect Ag sphere in free-space within the quasistatic limit ($d \lesssim 30$ nm) and schematic of surface charge distributions of selected LSPR modes. The energy difference between the l and $l + 1$ modes approaches zero as l approaches infinity. The density of states is dominated by a superposition of high-order modes, aggregating at 3.6 eV. The aggregated high l modes are referred to collectively as the quasiplanar mode (QP).

the plasmonic density of states of a perfect sphere in free-space within the quasistatic limit. Here, we see that the plasmon modes are bounded above by the standing wave SPP energy of a Ag-air planar interface (3.6 eV).[50−52] As l approaches infinity, the energy difference between the l and $l + 1$ modes approaches zero, causing the high l modes to aggregate around 3.6 eV. The aggregated high l modes become a single dominant peak due to line-width broadening and are referred to collectively as the quasiplanar (QP) mode[44] as they are associated with the

standing wave limit of the SPP. In contrast to the perfect sphere considered by Mie, the experiment presented here is performed on substrate-supported truncated spheres. In the following, we perform full-wave electrodynamics simulations to compare directly with the experiment and, where appropriate, use simulations to explore properties of the system inaccessible by the experiment.

While we examine a wide range of nanoparticle sizes, our discussion begins with the plasmonic spectrum of a $d = 85$ nm particle because it exhibits all the main spectral features observed in particles of other sizes. The experimental EEL spectrum for an aloof beam trajectory (red trace) is displayed in Figure 3a. Three major peaks are evident. The lowest-energy
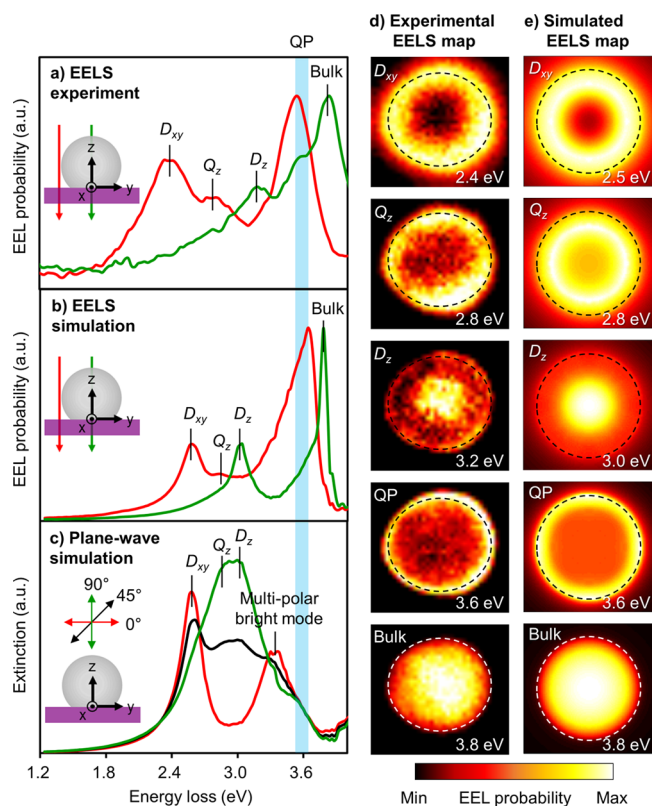

Figure 3. (a) Experimental EEL spectra, (b) simulated EEL spectra, and (c) simulated extinction spectra of a $d = 85$ nm Ag nanoparticle on a Si_3N_4 substrate. The aloof beam trajectory (red traces) are in close proximity to the particle edge, whereas the internal beam trajectory (green traces) are directed approximately though the center of the particle. The polarization angle dependence of the simulated extinction spectra is color coded: red for 0°, black for 45°, and green for 90°. (d) Experimental EELS maps for the LSPR modes: x,y-polarized dipole (D_{xy}, 2.4 eV), z-polarized quadrupole (Q_z, 2.8 eV), z-polarized dipole (D_z, 3.2 eV), quasiplanar (QP, 3.6 eV), and bulk modes (3.8 eV). (e) Simulated EELS maps for the LSPR modes in correspondence to those listed in (d). The outlines in both (d) and (e) trace the surface of the particle.

peak located at 2.4 eV (2.5 eV in simulation) are the dipole modes polarized parallel to the substrate, denoted as D_{xy}. As can be seen in the plane-wave simulations (Figure 3c), the D_{xy} modes are only excitable when the electric field of the incident light has a component parallel to the substrate. The corresponding D_{xy} EELS map (Figure 3d) is in excellent agreement with simulation (Figure 3e). The near-zero probability at the center of the D_{xy} EELS map is a signature

of the electron-probe imposed selection rules, which forbid the excitation of the D_{xy} mode from the center of the particle; that is, the radial symmetry of electron's electric field means that it cannot excite the intrinsically transverse D_{xy} mode, analogous to the inability of the electron beam to excite the super-radiant mode in the gap-region of a nanoparticle dimer system.[41,53]

We assign the peak located at 2.8 eV in both experiment and simulation to a quadrupole-like mode, Q_z, aligned perpendicular to the substrate.[28] Plane-wave simulations (Figure 3c) show that this mode is only excitable when the incident electric field has a component normal to the substrate, indicating that Q_z is polarized normal to the substrate, in agreement with previous studies.[28] The experimental and simulated EELS maps (Figure 3d and 3e) for the Q_z mode are only in qualitative agreement because Q_z is weakly excited in simulation and it lies on the blue shoulder of the D_{xy} peak, making the simulated EELS map at 2.8 eV a superposition of these two modes. A quadrupole-like mode polarized parallel to the substrate (Q_{xy}) has been reported to exist in truncated Ag nanospheres in the quantum size regime;[28] however, we do not observe this mode. This is most likely due to the low oscillator strength of this mode for particles within this size range.

At approximately 3.6 eV, the QP mode is the dominant feature in the EEL spectrum for all particle sizes probed with an aloof beam trajectory. The QP EELS map (Figure 3d and 3e) exhibits the strongest localization to the surface, indicating the high-order nature of the QP mode. To quantify this localization, Figure 4 plots the EEL probability at the D_{xy} and
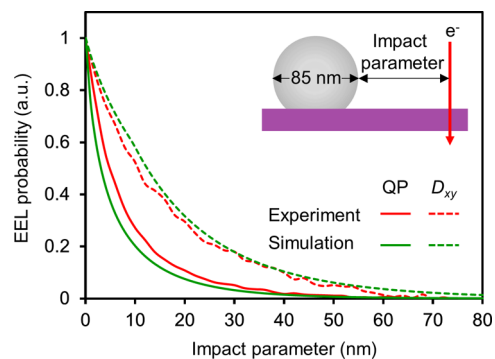

Figure 4. Experimental (red) and simulated (green) EEL probability at the D_{xy} and QP mode energies as a function of impact parameter for a $d = 85$ nm particle. The EEL probability at each of the mode energies is normalized to unity at the nanoparticle surface (impact parameter = 0 nm). The QP mode decays fastest with increasing distance between the electron beam and the particle surface, indicating that the QP mode is tightly bound to the surface.

QP mode energies as a function of impact parameter, that is, the distance between the beam and the particle surface. Both experimental and theoretical results show that the EEL probability at the QP mode energy decays fastest from the surface, indicating a high degree of surface localization. The simulated extinction spectra in Figure 3c shows that the QP mode cannot be excited by plane-wave light. This is also consistent with the interpretation of the QP mode as a standing wave SPP because momentum conservation forbids direct coupling between SPPs and plane-wave light.[52]

A broad peak located at 3.3 eV appears in the extinction spectra, suggesting the existence of an additional bright mode red-shifted from the QP mode. The insensitivity of this 3.3 eV mode to the polarization of the incident light is shown in Figure
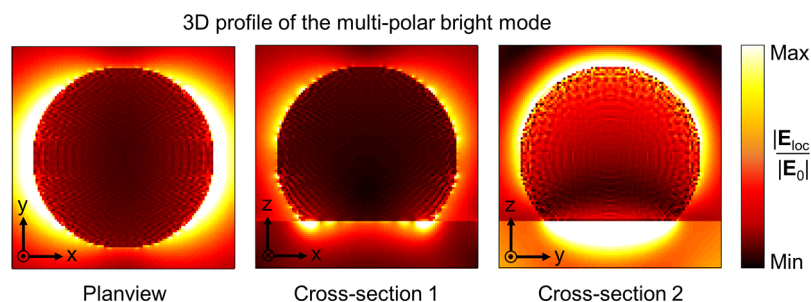
Figure 5. Simulated local electric-field magnitude, $|E_{loc}|$, of the multipolar bright mode, normalized to the incident electric field $|E_0|$. The incident plane-wave light is polarized parallel to the substrate (x axis) and propagating normal to the substrate (z axis). The view plane is indicated in the bottom left corner of each plot. Note the nodal structure of the electric field along the surface of particle, which indicates a multipolar character to this mode.
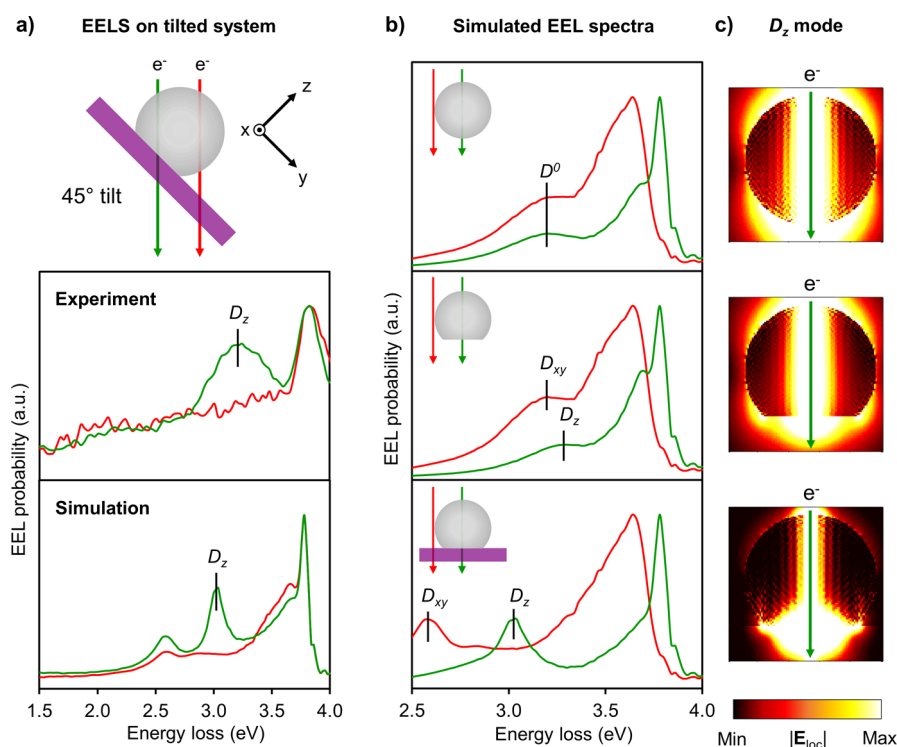

Figure 6. (a) Experimental and simulated EEL spectra of a 45° tilted particle–substrate system. The top panel is the schematic of the setup with two internal beam trajectories: one that intersects the particle–substrate interface and one that does not. Both experimental and simulated EEL spectra show that the D_z mode is only excited when the beam passes through the interface. (b) Simulated EEL spectra and (c) simulated local electric-field magnitudes of the D_z modes induced by internal beam trajectories for three systems; a perfect sphere in free-space (top panel), a truncated sphere in free-space (middle panel), and a truncated sphere on Si_3N_4 substrate (bottom panel). In the case of the perfect sphere in free space, the x,y,z-polarized dipole modes are energetically degenerate and are denoted as D^0. Aloof beam trajectories are chosen to excite the D_{xy} modes, whereas the internal beam trajectories are chosen to excite the D_z mode. The large local electric field magnitude that appears throughout the center of the particle is the local response of the metal to the passing electron beam.

3c, where the extinction spectra exhibit a resonance for all polarizations of light. The local electric field magnitude for x-polarized plane-wave excitation is presented in Figure 5 and exhibits multiple nodes along the surface of the particle, indicating the multipolar nature of this mode. Moreover, the existence of this mode explains the asymmetrical line shape in the EEL spectra near the QP mode (Figure 3a and b).

The experimental EEL spectra for the internal beam trajectory (green trace, Figure 3a) shows two major peaks. The resonance at 3.8 eV and corresponding EELS map serve as a control as it arises from the well-understood bulk-plasmon mode. The 3.2 eV (3.0 eV in simulation) mode is particularly interesting as it appears only for the internal beam trajectory

and has an EELS map that is concentrated toward the center of the particle. The 3D profile of this mode is determined by tilting the system 45° and acquiring EEL spectra for two separate internal beam trajectories: the first directed to pass through the Ag–Si$_3$N$_4$ interface and the second directed away from the interface (Figure 6a, top panel). We find that the mode at 3.2 eV is only excitable when the beam passes through the interface (Figure 6a, middle panel), indicating that this mode is confined to the particle–substrate interface, a feature well reproduced by our simulations (Figure 6a, bottom panel).

Comparing the simulated EEL spectra for a perfect sphere, a truncated sphere in free space, and a truncated sphere supported by a substrate allows us to deconvolve the effect of
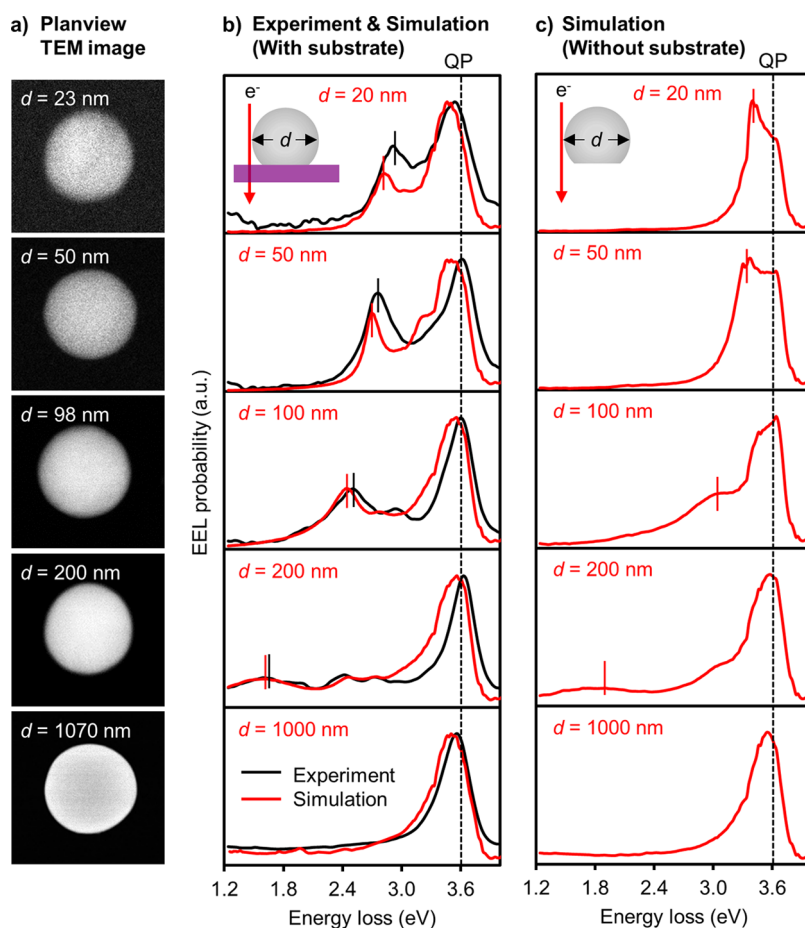
Figure 7. (a) Planview TEM (Z-contrast) images. (b) Experimental (black) and simulated (red) EEL spectra for truncated Ag spheres on a 30 nm thick Si_3N_4 substrate. In all cases, the electron beam most strongly interacts with the QP mode. (c) Simulated EEL spectra for truncated Ag spheres in free space with aloof beam trajectories. The electron beam preferentially interacts with the D_{xy} modes for 20 and 50 nm diameter particles, and with higher-order modes for 100, 200, and 1000 nm diameter particles. The D_{xy} and QP modes are labeled with a short vertical lines and a long dashed line, respectively.

truncation from that of the substrate on the origin of the 3.2 eV mode. For a perfect sphere in free space (Figure 6b, top panel), the x,y,z-polarized dipole modes are energetically degenerate and are denoted as D^0. The electric-field magnitude of the z-polarized dipole mode excited via an internal beam trajectory is shown in the top panel of Figure 6c and denoted as D_z. For a truncated sphere in free space (Figure 6b, middle panel), the simulation shows a blue shift of the D_z mode due to truncation of the sphere along the z axis. This is similar to the dipole energy splitting of a nanorod, where the dipole modes confined to the short axis are of higher energy than the dipole mode confined to the long axis.[54] The electric-field magnitude of the corresponding D_z mode, excited via a particle–substrate-intersecting trajectory still shows a characteristic dipole field (Figure 6c, middle panel) with the exception of an increased localization to the sharp edges and bottom face of the particle. Interestingly, this indicates that the D_z mode is only excitable through an internal beam trajectory in EELS. For a truncated sphere on a 30 nm thick Si_3N_4 substrate (bottom panel, Figure 6b), simulation shows a large redshift of all dipole modes, which is consistent with previous studies on substrate-dressed LSPR modes.[22] The electric-field magnitude displayed in the bottom panel of Figure 6c implies that the 3.2 eV (3.0 eV in simulation) peak observed in the experiment is a substrate-localized D_z mode. We also note a parallel between the D_z

mode observed here and the breathing modes observed in Ag nanodisks.[55]

Plane-wave simulations indicate that because D_z and Q_z are nearly degenerate and polarized in the same direction, far-field light can only excite a superposition of these modes. Contrastingly, EELS is uniquely capable of isolating the D_z mode because the electron beam can be directed to pass through the interface. Previous EELS studies,[43] however, have focused on aloof beam trajectories that, as we have shown, are blind to the D_z mode. The substrate-localized nature of the D_z mode makes it a good candidate for plasmonics applications where LSPR localization is thought to play an important role,[15] such as plasmon-enhanced PV[30,56] and photocatalysis,[18,33,57] plasmonic control of nanostructure morphology,[19,34] plasmon-induced nanoscale heating,[35] plasmon-enhanced photoelectron emission,[26] and Fano-induced loss reduction in plasmonic systems.[58]

With the above mode assignments in hand, we now investigate their dependence on particle size. Planview TEM images (Figure 7a) are correlated with experimental and simulated EEL spectra (Figure 7b) for aloof beam positions for particles with d = 23, 50, 98, 200, and 1070 nm. As the particle size increases, we observe the well-known redshifting and lifetime broadening of the LSPR modes. Interestingly, we find that the QP mode is the dominant feature in the EEL spectra

for all sizes and becomes the only discernible feature when $d = 1070$ nm. This is because the STEM electron interacts on the order of tens of nanometers (Figure 4) with the nanoparticle surface and when the radius of curvature of the surface is much larger than the interaction distance, the electron only "sees" a plane.

To isolate the substrate effect, we simulate EEL spectra for truncated Ag spheres in free space (Figure 7c). In contrast to what is observed in the experiment, we find that the electron preferentially interacts with low-order modes in free space, small-sized particles. However, as the particle diameter increases to the 50−100 nm range, the EEL spectra become QP mode dominated. The introduction of a Si_3N_4 substrate causes the QP mode to dominate the EEL spectra for particles as small as 20 nm as the substrate mediates the transfer of oscillator strength from the low-order to higher-order modes.[59] At large sizes ($d \gtrsim 200$ nm) the substrate effect is negligible because the electron effectively interacts with a free space Ag slab; therefore, the spectra for particles in free-space and those on a substrate become indistinguishable.

The spectra in Figure 7 are interpreted as a series of snapshots tracking the continuous evolution of an LSPR into an SPP. Though this has long been predicted by theory,[47,48] the ability to measure this effect is a testament to the power of EELS to probe the plasmonic spectrum of single nanoparticles, especially when combined with state-of-the-art synthesis. Moreover, the ultrasmooth nature of the PLiD-synthesized truncated nanospheres eliminates uncertainty about the nanoparticle geometry, allowing us to achieve excellent agreement between experiment and theory. For completeness, we also examine particles with sizes ranging from tens to hundreds of nanometers and the size-dependence of the D_{xy}, Q_z, D_z, and QP modes appears in Figure S1 (Supporting Information).

In this paper, we study the plasmonic spectrum of PLiD synthesized truncated Ag nanospheres over the nanometer-to-micron size regime using STEM/EELS and full-wave electrodynamics simulations. We provide the first nanoscale examination of substrate-induced LSPR mode splitting in truncated nanospheres and we present a near-field characterization of substrate-localized bright modes. We find that in the presence of a substrate, the STEM-electron preferentially interacts with the QP mode for particles as small as 20 nm in diameter. Additionally, the size-dependent study allows us to observe the evolution of an LSPR into a standing wave SPP, demonstrating the unique ability of STEM/EELS to resolve the complete plasmonic spectrum of nanoparticles. This work contributes to the fundamental understanding of the plasmonic properties of substrate-supported truncated nanospheres, facilitating the predictive engineering of PLiD-synthesized nanoparticles in plasmonics applications. This knowledge provides researchers with the tools necessary to develop a more detailed understanding of the interplay between particle morphology, size, substrate, and energy transfer in nanoparticle−substrate systems, with implications for improving the efficiency of plasmon-enhanced solar energy harvesting.

■ EXPERIMENTAL METHODS

Pulsed Laser-Induced Self-Assembly. Silver films of 18 and 35 nm in thicknesses are sputter-deposited on 30 nm silicon nitride TEM substrates using a radio frequency (RF) magnetron source. The measured sputtering rate for Ag is 3 nm/min using the following sputtering conditions: 5 cm diameter sputter target, a forward RF power of 20 W, 25 sccm Ar at 5 mTorr processing pressure, and a 100 V self-bias is applied to the substrate. Subsequently, a KrF 18 ns pulsed excimer laser at 248 nm wavelength is used to melt the Ag films with two laser pulses at a fluence of 60 mJ/cm². Arrays of truncated spherical nanoparticles spanning from nanometers to microns in size are then formed from the melt Ag films.

Ag Dielectric Function Measurement. An optically thick 250 nm-thick Ag film deposited on a silicon nitride coated Si wafer is used for dielectric function measurement. The dielectric function for Ag film are measured using a J.A. Woolam M-2000U variable angle spectroscopic ellipsometer over a wavelength of 245−999 nm. To fit the raw data, the film is represented as a slab of uniform thickness having sharp interfaces and optical properties described by the Cauchy model. The best fit is achieved using a point by point regression analysis to minimize the mean squared error. The measured dielectric function can be found in Figure S2 of the Supporting Information. For consistency, the commonly used Johnson and Christy (JC) data[60] is also included in Figure S2.

EELS Experiments. EELS experiments are carried out in a monochromated Carl Zeiss LIBRA 200MC (S)TEM operated at 200 kV. All spectrum acquisitions are performed with a convergence semiangle of 9 mrad, a collection semiangle of 12 mrad, a dispersion of 29 meV per channel. The measured energy resolution (defined as the full width at half-maximum of the zero-loss peak) is 150 meV with the electron beam penetrating the Si_3N_4 substrate only. This spectrum serves as the background for posterior data processing. For the $d = 85$ nm particle, two EEL spectrum images are acquired: (1) one is used for generating LSPR mode maps and (2) the other is used for plotting plasmon decay as a function of impact parameter. For spectrum image (1), a region of interest (ROI) with 34 × 32 pixel spectra (1 pixel ∼3.3 nm × 3.3 nm) is defined over the whole Ag nanoparticle. For spectrum image (2), a ROI with 38 × 7 pixel spectra (1 pixel ∼2.0 nm × 2.0 nm) starting from the particle surface is chosen along the radial direction of the nanosphere. The impact parameter is divided into 38 steps, with each step measuring 2 nm in length and containing 7 pixel spectra. For particles of other sizes, only aloof and internal beam trajectories are used to obtain point spectra.

Data Processing. The point EEL spectra are normalized and the background spectrum is subtracted. The subsequent spectra are used to compare with the theoretical simulations. To generate the LSPR maps, the background of all pixel spectra are removed through the reflected-tail model routine using the Gatan "Digital Micrograph" software, and then normalize pixel by pixel by the zero-loss intensity. Finally, by plotting the spectral intensities in designated energy slices, the LSPR maps are generated. To plot the plasmon decay as a function of impact parameter, the spectral intensity of a particular LSPR mode in each of the 38 steps are extracted and plotted as a function of distance away from the surface. The plot shown in Figure 4 is normalized to the EEL probability of each mode obtained at the surface (impact parameter = 0 nm).

EELS Simulations. For the purpose of directly modeling the experiment, computational results were produced using the coupled-dipole[61] or discrete dipole approximation (DDA) approach,[40] which is routinely used to study the response of metal nanoparticles subjected to far-field optical-frequency radiation. We have previously developed and numerically implemented the electron-driven discrete-dipole approximation (e-DDA)[41,42] as a generalization of the DDA, incorporating the

electron beam of a STEM in place of a plane-polarized electric-field source. Both aloof and internal electron beam trajectories are computed using the same code base. Dipole spacing was variable and chosen such that the simulations converged for all observables presented. All electron beams were assumed to be perpendicular to the substrate (if present), unless explicitly stated otherwise and all beam kinetic energies were 200 keV. All dielectric data was taken from our ellipsometry experiments, except for that of the substrate material, amorphous silicon nitride, which was taken from the literature.[62]

ASSOCIATED CONTENT

Ⓢ Supporting Information

(i) Size-dependence of LSPR modes, (ii) measured Ag dielectric function compared to JC data, and (iii) references containing more than 10 authors. The Supporting Information is available free of charge on the ACS Publications website at DOI: 10.1021/acs.jpclett.5b00961.

AUTHOR INFORMATION

Corresponding Authors

*E-mail: masiello@chem.washington.edu (D.J.M.).
*E-mail: jon.camden@nd.edu (J.P.C.).

Author Contributions

¶(G.L., C.C.) These authors contributed equally to this work.

Notes

The authors declare no competing financial interest.

ACKNOWLEDGMENTS

REFERENCES

(1) Nie, S.; Emory, S. R. Probing Single Molecules and Single Nanoparticles by Surface-Enhanced Raman Scattering. *Science* **1997**, *275*, 1102−1106.

(2) Schlücker, S. Surface-Enhanced Raman Spectroscopy: Concepts and Chemical Applications. *Angew. Chem., Int. Ed.* **2014**, *53*, 4756−4795.

(3) Quinten, M.; Leitner, A.; Krenn, J. R.; Aussenegg, F. R. Electromagnetic Energy Transport via Linear Chains of Silver Nanoparticles. *Opt. Lett.* **1998**, *23*, 1331−1333.

(4) Clavero, C. Plasmon-Induced Hot-Electron Generation at Nanoparticle/Metal-Oxide Interfaces for Photovoltaic and Photo-catalytic Devices. *Nat. Photonics* **2014**, *8*, 95−103.

(5) Atwater, H. A.; Polman, A. Plasmonics for Improved Photovoltaic Devices. *Nat. Mater.* **2010**, *9*, 205−213.

(6) Mubeen, S.; Lee, J.; Liu, D.; Stucky, G. D.; Moskovits, M. Panchromatic Photoproduction of H_2 with Surface Plasmons. *Nano Lett.* **2015**, *15*, 2132−2136.

(7) Chen, H. M.; Chen, C. K.; Chen, C.-J.; Cheng, L.-C.; Wu, P. C.; Cheng, B. H.; Ho, Y. Z.; Tseng, M. L.; Hsu, Y.-Y.; Chan, T.-S.; et al. Plasmon Inducing Effects for Enhanced Photoelectrochemical Water Splitting: X-ray Absorption Approach to Electronic Structures. *ACS Nano* **2012**, *6*, 7362−7372.

(8) Ozbay, E. Plasmonics: Merging Photonics and Electronics at Nanoscale Dimensions. *Science* **2006**, *311*, 189−193.

(9) Fleischmann, M.; Hendra, P. J.; McQuillan, A. J. Raman Spectra of Pyridine Adsorbed at a Silver Electrode. *Chem. Phys. Lett.* **1974**, *26*, 163−166.

(10) Jönsson, U.; Fägerstam, L.; Ivarsson, B.; Johnsson, B.; Karlsson, R.; Lundh, K.; Löfas, S.; Persson, B.; Roos, H.; Rönnberg, I.; et al. Real-Time Biospecific Interaction Analysis Using Surface Plasmon Resonance and A Sensor Chip Technology. *BioTechniques* **1991**, *11*, 620−7.

(11) Takahara, J.; Yamagishi, S.; Taki, H.; Morimoto, A.; Kobayashi, T. Guiding of A One-Dimensional Optical Beam with Nanometer Diameter. *Opt. Lett.* **1997**, *22*, 475−7.

(12) Ebbesen, T. W.; Lezec, H. J.; Ghaemi, H. F.; Thio, T.; Wolff, P. A. Extraordinary Optical Transmission Through Sub-Wavelength Hole Arrays. *Nature* **1998**, *391*, 667−669.

(13) Pendry, J. B. Negative Refraction Makes a Perfect Lens. *Phys. Rev. Lett.* **2000**, *85*, 3966−3969.

(14) Focusing in on applications. *Nat. Nanotechnol.* **2015**, *10*, 1−1.

(15) Li, G.; Cherqui, C.; Bigelow, N. W.; Duscher, G.; Straney, P. J.; Millstone, J. E.; Masiello, D. J.; Camden, J. P. Spatially Mapping Energy Transfer from Single Plasmonic Particles to Semiconductor Substrates via STEM/EELS. *Nano Lett.* **2015**, *15*, 3465−3471.

(16) Li, J.; Cushing, S. K.; Bright, J.; Meng, F.; Senty, T. R.; Zheng, P.; Bristow, A. D.; Wu, N. Ag@Cu_2O Core-Shell Nanoparticles as Visible-Light Plasmonic Photocatalysts. *ACS Catal.* **2012**, *3*, 47−51.

(17) Cushing, S. K.; Li, J.; Meng, F.; Senty, T. R.; Suri, S.; Zhi, M.; Li, M.; Bristow, A. D.; Wu, N. Photocatalytic Activity Enhanced by Plasmonic Resonant Energy Transfer from Metal to Semiconductor. *J. Am. Chem. Soc.* **2012**, *134*, 15033−15041.

(18) Li, J.; Cushing, S. K.; Zheng, P.; Meng, F.; Chu, D.; Wu, N. Plasmon-Induced Photonic and Energy-Transfer Enhancement of Solar Water Splitting by A Hematite Nanorod Array. *Nat. Commun.* **2013**, *4*, 2651.

(19) Tanabe, I.; Tatsuma, T. Plasmonic Manipulation of Color and Morphology of Single Silver Nanospheres. *Nano Lett.* **2012**, *12*, 5418−5421.

(20) Furube, A.; Du, L.; Hara, K.; Katoh, R.; Tachiya, M. Ultrafast Plasmon-Induced Electron Transfer from Gold Nanodots into TiO_2 Nanoparticles. *J. Am. Chem. Soc.* **2007**, *129*, 14852−14853.

(21) Hoggard, A.; Wang, L.-Y.; Ma, L.; Fang, Y.; You, G.; Olson, J.; Liu, Z.; Chang, W.-S.; Ajayan, P. M.; Link, S. Using the Plasmon Linewidth To Calculate the Time and Efficiency of Electron Transfer between Gold Nanorods and Graphene. *ACS Nano* **2013**, *7*, 11209−11217.

(22) Ringe, E.; McMahon, J. M.; Sohn, K.; Cobley, C.; Xia, Y.; Huang, J.; Schatz, G. C.; Marks, L. D.; Van Duyne, R. P. Unraveling the Effects of Size, Composition, and Substrate on the Localized Surface Plasmon Resonance Frequencies of Gold and Silver Nanocubes: A Systematic Single-Particle Approach. *J. Phys. Chem. C* **2010**, *114*, 12511−12516.

(23) Scholl, J. A.; Koh, A. L.; Dionne, J. A. Quantum Plasmon Resonances of Individual Metallic Nanoparticles. *Nature* **2012**, *483*, 421−U68.

(24) Yamamoto, N.; Ohtani, S.; García de Abajo, F. J. Gap and Mie Plasmons in Individual Silver Nanospheres near a Silver Surface. *Nano Lett.* **2010**, *11*, 91−95.

(25) Hung, L.; Lee, S. Y.; McGovern, O.; Rabin, O.; Mayergoyz, I. Calculation and Measurement of Radiation Corrections for Plasmon Resonances in Nanoparticles. *Phys. Rev. B* **2013**, *88*, 075424.

(26) Grubisic, A.; Ringe, E.; Cobley, C. M.; Xia, Y.; Marks, L. D.; Van Duyne, R. P.; Nesbitt, D. J. Plasmonic Near-Electric Field Enhancement Effects in Ultrafast Photoelectron Emission: Correlated Spatial and Laser Polarization Microscopy Studies of Individual Ag Nanocubes. *Nano Lett.* **2012**, *12*, 4823−4829.

(27) Lazzari, R.; Simonsen, I. GranFilm: A Software for Calculating Thin-Layer Dielectric Properties and Fresnel Coefficients. *Thin Solid Films* **2002**, *419*, 124−136.

(28) Lazzari, R.; Jupille, J.; Cavallotti, R.; Simonsen, I. Model-Free Unraveling of Supported Nanoparticles Plasmon Resonance Modes. *J. Phys. Chem. C* **2014**, *118*, 7032−7048.

(29) Takahashi, Y.; Tatsuma, T. Solid State Photovoltaic Cells Based on Localized Surface Plasmon-Induced Charge Separation. *Appl. Phys. Lett.* **2011**, *99*, 182110.

(30) Kawawaki, T.; Takahashi, Y.; Tatsuma, T. Enhancement of Dye-Sensitized Photocurrents by Gold Nanoparticles: Effects of Plasmon Coupling. *J. Phys. Chem. C* **2013**, *117*, 5901−5907.

(31) Tian, Y.; Notsu, H.; Tatsuma, T. Visible-Light-Induced Patterning of Au- and Ag-TiO$_2$ Nanocomposite Film Surfaces on the Basis of Plasmon Photoelectrochemistry. *Photochem. Photobiol. Sci.* **2005**, *4*, 598−601.

(32) Yamaguchi, T.; Kazuma, E.; Sakai, N.; Tatsuma, T. Photo-electrochemical Responses from Polymer-Coated Plasmonic Copper Nanoparticles on TiO$_2$. *Chem. Lett.* **2012**, *41*, 1340−1342.

(33) Konishi, Y.; Tanabe, I.; Tatsuma, T. Stable Spectral Dip Formation and Multicolour Changes of Plasmonic Gold Nanoparticles on TiO$_2$. *Chem. Commun.* **2013**, *49*, 606−608.

(34) Matsubara, K.; Tatsuma, T. Morphological Changes and Multicolor Photochromism of Ag Nanoparticles Deposited on Single-Crystalline TiO$_2$ Surfaces. *Adv. Mater.* **2007**, *19*, 2802−2806.

(35) Setoura, K.; Okada, Y.; Werner, D.; Hashimoto, S. Observation of Nanoscale Cooling Effects by Substrates and the Surrounding Media for Single Gold Nanoparticles under CW-Laser Illumination. *ACS Nano* **2013**, *7*, 7874−7885.

(36) Wu, Y.; Dong, N.; Fu, S.; Fowlkes, J. D.; Kondic, L.; Vincenti, M. A.; de Ceglia, D.; Rack, P. D. Directed Liquid Phase Assembly of Highly Ordered Metallic Nanoparticle Arrays. *ACS Appl. Mater. Interfaces* **2014**, *6*, 5835−5843.

(37) Wu, Y.; Fowlkes, J. D.; Roberts, N. A.; Diez, J. A.; Kondic, L.; González, A. G.; Rack, P. D. Competing Liquid Phase Instabilities during Pulsed Laser Induced Self-Assembly of Copper Rings into Ordered Nanoparticle Arrays on SiO$_2$. *Langmuir* **2011**, *27*, 13314−13323.

(38) McKeown, J. T.; Wu, Y.; Fowlkes, J. D.; Rack, P. D.; Campbell, G. H. Simultaneous In-Situ Synthesis and Characterization of Co@Cu Core-Shell Nanoparticle Arrays. *Adv. Mater.* **2015**, *27*, 1060−1065.

(39) Trice, J.; Thomas, D.; Favazza, C.; Sureshkumar, R.; Kalyanaraman, R. Pulsed-Laser-Induced Dewetting in Nanoscopic Metal Films: Theory and Experiments. *Phys. Rev. B* **2007**, *75*, 235439.

(40) Draine, B. T.; Flatau, P. J. Discrete-Dipole Approximation for Scattering Calculations. *J. Opt. Soc. Am. A* **1994**, *11*, 1491−1499.

(41) Bigelow, N. W.; Vaschillo, A.; Iberi, V.; Camden, J. P.; Masiello, D. J. Characterization of the Electron- and Photon-Driven Plasmonic Excitations of Metal Nanorods. *ACS Nano* **2012**, *6*, 7497−7504.

(42) Bigelow, N. W.; Vaschillo, A.; Camden, J. P.; Masiello, D. J. Signatures of Fano Interferences in the Electron Energy Loss Spectroscopy and Cathodoluminescence of Symmetry-Broken Nano-rod Dimers. *ACS Nano* **2013**, *7*, 4511−4519.

(43) Ouyang, F.; Batson, P. E.; Isaacson, M. Quantum Size Effects in the Surface-Plasmon Excitation of Small Metallic Particles by Electron-Energy-Loss Spectroscopy. *Phys. Rev. B* **1992**, *46*, 15421−15425.

(44) Aizpurua, J.; Rivacoba, A.; Apell, S. P. Electron-Energy Losses in Hemispherical Targets. *Phys. Rev. B* **1996**, *54*, 2901−2909.

(45) Pennycook, S. J.; Varela, M.; Lupini, A. R.; Oxley, M. P.; Chisholm, M. F. Atomic-Resolution Spectroscopic Imaging: Past, Present and Future. *J. Electron Microsc.* **2009**, *58*, 87−97.

(46) Nicoletti, O.; de la Pena, F.; Leary, R. K.; Holland, D. J.; Ducati, C.; Midgley, P. A. Three-Dimensional Imaging of Localized Surface Plasmon Resonances of Metal Nanoparticles. *Nature* **2013**, *502*, 80−84.

(47) Mie, G. Articles on the Optical Characteristics of Turbid Tubes, Especially Colloidal Metal Solutions. *Ann. Phys.* **1908**, *25*, 377−445.

(48) Kliewer, K. L.; Fuchs, R. Theory of Dynamical Properties of Dielectric Surfaces. In *Adv. Chem. Phys.*; John Wiley & Sons, Inc.: Hoboken, NJ, 1974; pp 355−541.

(49) Economou, E. N.; Ngai, K. L. Surface Plasma Oscillations and Related Surface Effects in Solids. In *Adv. Chem. Phys.*; John Wiley & Sons, Inc.: Hoboken, NJ, 1974; pp 265−354.

(50) Chen, J.; Smolyakov, G. A.; Brueck, S. R.; Malloy, K. J. Surface Plasmon Modes of Finite, Planar, Metal-Insulator-Metal Plasmonic Waveguides. *Opt. Express* **2008**, *16*, 14902−14909.

(51) Dionne, J. A.; Sweatlock, L. A.; Atwater, H. A.; Polman, A. Planar Metal Plasmon Waveguides: Frequency-Dependent Dispersion, Propagation, Localization, and Loss Beyond the Free Electron Model. *Phys. Rev. B* **2005**, *72*, 075405.

(52) Pitarke, J. M.; Silkin, V. M.; Chulkov, E. V.; Echenique, P. M. Theory of Surface Plasmons and Surface-Plasmon Polaritons. *Rep. Prog. Phys.* **2007**, *70*, 1.

(53) Mirsaleh-Kohan, N.; Iberi, V.; Simmons, P. D., Jr.; Bigelow, N. W.; Vaschillo, A.; Rowland, M. M.; Best, M. D.; Pennycook, S. J.; Masiello, D. J.; Guiton, B. S.; et al. Single-Molecule Surface-Enhanced Raman Scattering: Can STEM/EELS Image Electromagnetic Hot Spots? *J. Phys. Chem. Lett.* **2012**, *3*, 2303−2309.

(54) Guiton, B. S.; Iberi, V.; Li, S.; Leonard, D. N.; Parish, C. M.; Kotula, P. G.; Varela, M.; Schatz, G. C.; Pennycook, S. J.; Camden, J. P. Correlated Optical Measurements and Plasmon Mapping of Silver Nanorods. *Nano Lett.* **2011**, *11*, 3482−3488.

(55) Schmidt, F.-P.; Ditlbacher, H.; Hohenester, U.; Hohenau, A.; Hofer, F.; Krenn, J. R. Dark Plasmonic Breathing Modes in Silver Nanodisks. *Nano Lett.* **2012**, *12*, 5780−5783.

(56) Veenkamp, R. J.; Ye, W. N. Plasmonic Metal Nanocubes forBroadband Light Absorption Enhancement in Thin-Film a-Si Solar Cells. *J. Appl. Phys.* **2014**, *115*, 124317.

(57) Linic, S.; Christopher, P.; Xin, H.; Marimuthu, A. Catalytic and Photocatalytic Transformations on Metal Nanoparticles with Targeted Geometric and Plasmonic Properties. *Acc. Chem. Res.* **2013**, *46*, 1890−1899.

(58) Gallinet, B.; Martin, O. J. F. Refractive Index Sensing with Subradiant Modes: A Framework to Reduce Losses in Plasmonic Nanostructures. *ACS Nano* **2013**, *7*, 6978−6987.

(59) Zhang, S.; Bao, K.; Halas, N. J.; Xu, H.; Nordlander, P. Substrate-Induced Fano Resonances of a Plasmonic Nanocube: A Route to Increased-Sensitivity Localized Surface Plasmon Resonance Sensors Revealed. *Nano Lett.* **2011**, *11*, 1657−1663.

(60) Johnson, P. B.; Christy, R. W. Optical Constants of the Noble Metals. *Phys. Rev. B* **1972**, *6*, 4370−4379.

(61) Purcell, E. M.; Pennypacker, C. R. Scattering and Absorption of Light by Nonspherical Dielectric Grains. *Astrophys. J.* **1973**, *186*, 705−714.

(62) Lide, D. R. Properties of Solids. In *CRC Handbook of Chemistry and Physics*, 95th ed.; CRC Press: Boca Raton, FL, 2005; pp 171−172.